Phenomenological approaches for quantitative temperature-programmed reduction (TPR) and desorption (TPD) analysis

Simoní Da Ros, Karen Aline Valter Flores, Marcio Schwaab, Elisa Barbosa-Coutinho, Nádia R.C. Fernandes, José Carlos Pinto

PII: S1226-086X(20)30527-X

DOI: https://doi.org/10.1016/j.jiec.2020.11.018

Reference: JIEC 5299

To appear in: *Journal of Industrial and Engineering Chemistry*

Received Date: 1 September 2020

Revised Date: 1 November 2020

Accepted Date: 21 November 2020

Please cite this article as: { doi: https://doi.org/

Phenomenological approaches for quantitative temperature-programmed reduction (TPR) and desorption (TPD) analysis

Simoní Da Ros[1*], Karen Aline Valter Flores[2], Marcio Schwaab[2], Elisa Barbosa-Coutinho[3], Nádia R, C. Fernandes[4], José Carlos Pinto[5]

[1 -] UCL Institute for Sustainable Heritage, University College London, 14 Upper Woburn Place, London WC1H 0NN

[2 -] Departamento de Engenharia Química, Escola de Engenharia, Universidade Federal do Rio Grande do Sul. Rua Ramiro Barcelos, 2777, Prédio 22202, Porto Alegre, RS, 90035-007, Brasil.

[3] - Departamento de Físico-Química, Instituto de Química, Universidade Federal do Rio Grande do Sul. Av. Bento Gonçalves, 9500, Porto Alegre, RS, 91501-970, Brasil.

[4 -] Departamento de Engenharia Química, Universidade Estadual de Maringá, Av. Colombo, 5790, Cidade Universitária, Maringá, PR, 87020-900, Brasil.

[5 -] Programa de Engenharia Química/COPPE, Universidade Federal do Rio de Janeiro. Cidade Universitária - CP: 68502, Rio de Janeiro, RJ, 21941-972, Brasil.

* Corresponding author: s.ros@ucl.ac.uk

Graphical abstract

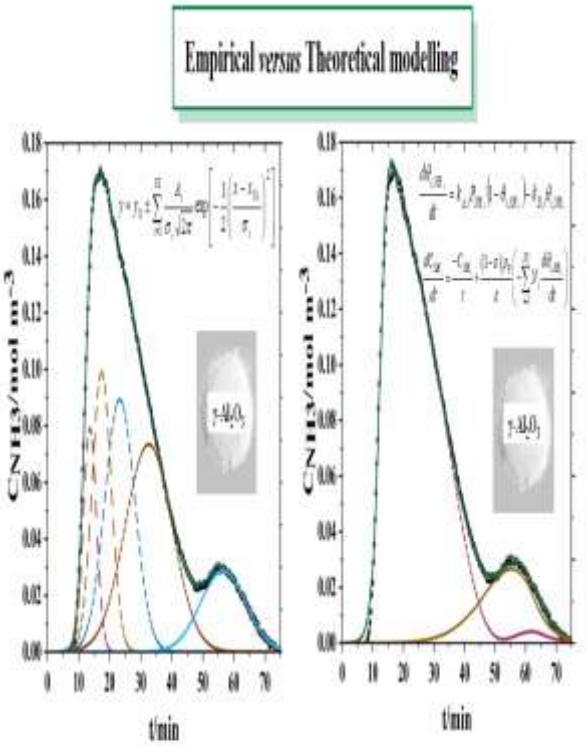

Abstract

Temperature-programmed reduction (TPR) and temperature-programmed desorption (TPD) are techniques widely used for catalyst characterization, providing information about active sites. However, results from these experiments are usually interpreted with the aid of empirical models, based on the representation of reduction or desorption profiles as summations of empirical reference curves. In this context, phenomenological approaches can present several advantages over this traditional empirical approach, as in this case the extracted information can be based on theoretical models that allows for a deeper understanding of the catalyst properties. For this reason, in the present work, empirical and phenomenological modelling approaches are evaluated for the quantitative analysis of H_2-TPR and NH_3-TPD profiles, obtained from the characterization of Ni/SiO_2 and Al_2O_3 alumina catalysts, respectively, and results from both approaches are thoroughly compared and discussed for the first time. Our results, obtained from the fitting of both modelling approaches to the whole experimental profile by using nonlinear regression, indicate that the phenomenological modelling approach can be considered better and should therefore be preferred, as it allows for significantly more accurate quantification and correct discrimination of distinct active sites, in addition to simultaneously enabling the determination of reduction or desorption kinetics parameters.

Keywords: heterogeneous catalysts; temperature-programmed reduction; temperature-programmed desorption; curve deconvolution; parameter estimation; nonlinear regression.

Introduction

Thermoanalytical techniques are often associated with transient characterization methods that are designed to monitor certain sample properties as functions of time, usually accompanied by the simultaneous increase of temperature [1–3], allowing the acquisition of significant amount of information about the analyzed material properties in a short period of time. These thermonalytical techniques have been widely applied in several fields, like the investigation of the thermal stability and thermal and mechanical properties of polymers [4] and the characterization of heterogenous catalysts [5–8].

In the field of heterogenous catalysis, monitoring of some specific catalyst properties, such as the number of acidic, basic or metallic active sites, may constitute a step of paramount importance for development of optimized catalysts, which can allow the maximization of the yields of products of interest. In addition, the characterization of these (and possibly other) properties can also be fundamental for development of mathematical kinetic models required for the design, control and optimization of industrial reactors [9].

In this context, temperature-programmed (TP) techniques play a unique role, as they may allow for characterization of catalyst properties and assessment of the physico-chemical interactions that take place between the catalyst surface and the reactive species [2,10]. Among the many available TP techniques, Temperature-Programmed Reduction (TPR), Temperature-Programmed Desorption (TPD), Temperature-Programmed Oxidation (TPO) and Temperature-Programmed Surface Reaction (TPSR) are of particular importance. Whereas the evaluation of bulk oxygen mobility in catalysts (such as nanostructured ceria [11] and other metal catalysts [12–14]) can be performed through standard TPR analyses, which normally make use of gaseous H_2 streams as the reducing agent, the characterization of acid, basic and metallic sites can

frequently be carried out through TPD analyses, which make use of probe molecules (such as NH_3, CO_2 and H_2) that can adsorb onto and subsequently desorb from catalyst sites located on the catalyst surfaces [7,15,16]. Moreover, the evaluation of the extent of coke deposition on the catalyst surfaces can be evaluated through TPO analyses, which usually make use of O_2 streams as oxidizing agents [17,18], whereas interactions between the catalyst surfaces and the reactive species can be evaluated through TPSR analyses [1].

Nevertheless, despite the intensive and ample use of TP techniques for characterization of heterogeneous catalysts, the proper interpretation of the obtained thermograms still constitutes a challenge, as measured thermograms may depend not only on the catalyst properties, but also on the experimental conditions employed in the TP runs, such as the catalyst mass, gas flow rate, feed concentration of the reacting/probe molecule and temperature program [19–21].

The quantification of the number of reducible metallic species, acid, basic or metallic sites usually involves the calculation of the integral over time (or temperature) of intensities of the monitored TP signal during the thermoanalytical experiment, as the number of sites of a particular nature is expected to be proportional to the amount of consumed reducing agent, in the case of TPR analyses, or desorbed probe molecules, in the case of TPD analyses [21,22]. However, when two or more peaks are present in the TP thermogram, there may be an indication that the catalyst can contain sites with distinct characteristics, with more than one type of reducible species or active site (acid, basic or metallic) [10]. Since TPR and TPD experiments lead to transient responses, peaks related to distinct active species can be partially or highly overlapped, making the determination of the number of different types of catalyst sites and their relative quantities difficult or unfeasible [10,12,15]. Hopefully, in some cases it may be possible to separate the overlapped peaks through manipulation of the experimental TP conditions, although it is not always obvious how operation conditions should be changed to achieve this

result. As a consequence, it may be necessary to perform additional experiments for efficient peak resolution, rendering the experimental procedure more expensive and time consuming [21].

A strategy that has been frequently used in the literature to resolve overlapping peaks in a thermogram is deconvolution (although a more appropriate term should be *"curve decomposition"*, since *"deconvolution"* is a term used to describe a set of more complex and well-defined mathematical procedures [23]), which assumes that the obtained multimodal thermogram can be represented as the sum of simpler unimodal curves, after adjustment of some suitable parameters. Functions that are employed very frequently in deconvolution procedures resemble probability distribution functions like the Gaussian curve, which is unimodal, bi-parametric and symmetrical around its point of maximum. Nevertheless, any family of curves, in principle, could be considered in the decomposition procedure [24]. After curve fitting, the point of maximum, the peak width and the area beneath the individual curves can be calculated for each element of the sum. Usually, the number of curves needed to provide the appropriate fitting for the experimental thermogram is assumed to be equal to the number of distinct active species, whereas the relative area generated by each individual curve is regarded to provide a measure of the relative importance (quantity) of that site. As a matter of fact, curve deconvolution (or decomposition) has been widely used for TPD and TPR quantitative analyses [25–30]. Given the simplicity of the proposed empirical numerical approach, the use of deconvolution procedures seems appealing, despite the complete lack of phenomenological basis to support the use of the vast majority of available statistical functions to describe either the reduction or the desorption processes. Besides, it must be emphasized that there is no formal guarantee that the number of adjusted Gaussian curves, used to fit the TP thermogram, can indeed correspond to the actual number of distinct active species present in the catalyst.

An interesting alternative to the deconvolution procedure consists in modelling TP experiments with some sort of phenomenological approach. For instance, mass balance equations coupled with adsorption/desorption rate equations can be used to model the gas-phase concentration of the probe molecule in TPD analysis, allowing the determination of the number of types of active species and their relative quantities [15,31,32]. Similarly, mass balance equations can be coupled with reduction reaction rate equations in order to model the gas-phase concentration of the reducing agent in TPR experiments, allowing the quantification of the number of distinct reducible active sites and their relative amounts [14,33,34]. Moreover, besides allowing the quantitative characterization of the active species, the use of a phenomenological approach can also provide additional information about the kinetic rate parameters involved in the reduction or desorption reactions, such as the specific kinetic rate constants and the activation energies [31,32], which can constitute a very significant advantageous aspect of this type of mathematical representation of TP experiments.

Phenomenological approaches can also allow for specific model improvements, for instance, selection of appropriate desorption or reduction reaction rates or consideration of activation energy as a function of surface coverage and simultaneous estimation of the parameters of this function in order to achieve a better description of the experimental data [35]. Moreover, advanced experimental and chemical modelling techniques can be readily applied, such as DFT coupled microkinetic modelling [36], modelling CO-TPD profile with mean-field techniques and kinetic Monte Carlo allowing for the observation of lateral interactions among probe molecules [37] and coupled NH_3 temperature-programmed desorption with thermogravimetry for acid sites quantification in zeolites [38].

In this context, numerical methods have been proposed to perform quantitative kinetic analyses of thermograms, involving the definition of the points of maximum of modes of

thermograms collected at different heating rates [39–42]. However, although the use of these methods can seem appealing, as they require the fitting of simple straight-lines to provide the relative amounts and main characteristics of the individual catalyst sites, they present the drawback of reducing the entire thermogram profile to a small set of points while completely disregarding the full shape of the thermogram. For these reasons, numerical approaches that take into account the complete thermogram information should be preferred, as they can allow more meaningful characterization of the active species and the kinetics of desorption or reduction processes [12,14].

Based on the previous paragraphs, the present study evaluates - for the first time - the use of phenomenological mathematical approaches for the quantitative characterization of heterogeneous catalysts using TPR and TPD experiments when compared to empirical deconvolution methods of analysis. To do this, we use the reducible characteristics of a Ni/SiO_2 catalyst, as assessed by H_2-TPR, and the acid features of an Al_2O_3 alumina catalyst, as evaluated by NH_3-TPD experiments, and fit both modelling approaches to the experimental profiles by using nonlinear regression. In both cases, results from both analysis approaches are thoroughly compared and discussed. Our results indicate that the phenomenological modelling approach can be considered better and should therefore be preferred, as it allows for more accurate quantification and correct discrimination of distinct active sites, in addition to simultaneously enabling the determination of reduction or desorption kinetics parameters.

Materials and methods

H_2-TPR experimental procedure

All experimental TPR profiles were compiled from [13,43,44]. Nickel supported on silica catalyst (Ni/SiO_2) was prepared through the well-known deposition-precipitation method, as

described elsewhere [13,43,44]. The silica used as support consisted of a diatomaceous earth, with 1% of alumina, a specific surface area of 42 m^2/g and pore volume of 1.1 cm^3/g [13]. A slurry containing silica and nickel nitrate solution, which was used as active precursor, was kept at 90 ºC under agitation, while a 0.8M $NaHCO_3$ solution was added to promote nickel precipitation. The material was filtered, washed and dried at 200 ºC for 20 hours. Then the dried material was thermally treated at 200 ºC for 3 hours and then at 450 ºC for 2 hours. Nickel content of catalyst (NiO/SiO_2) was measured by atomic absorption spectroscopy (Perkin Elmer 1100B) and was equal to 40.7 wt.%. Specific surface area was equal to 57 m^2/g and measured by N_2 adsorption at 77 K (Micromeritics, ASAP2000), considering BET isotherm [43].

For the TPR analysis, the catalyst sample was pre-treated *in situ* under argon flow (30 mL/min) at 120 ºC for 30 minutes before exposition to the gas feed, which consisted of a 1.64 vol% H_2/Ar mixture flowing at 20 mL/min. In the sequence, the sample was heated up to 750 °C at heating rate of 5 ºC/min. Exhaust gases were analyzed with a thermal conductivity detector to quantify the H_2 concentration after the removal of water produced by the oxide reduction. Water removal was performed by flowing the gas stream through a silica-gel packed-bed. All TPR experiments were performed in a SAMP3 system (Termolab Equipamentos, Brazil) [43]. A good experimental reproducibility of the TPR experimental setup was confirmed by four replicated experiments, as illustrated in Fig. S1 of the Supplementary Information (*SI*) [43].

NH_3-TPD experimental procedure

Alumina catalysts were prepared and NH_3-TPD analysis performed as described elsewhere [6,45]. Aluminum hydroxide was precipitated from a solution of aluminum nitrate (100 g of $Al(NO_3)_3.9H_2O$ (Vetec, 98%) in 200 mL of deionized water) by dropwise addition of ammonium hydroxide solution (NH_4OH, 28 wt.%) until the solution pH was equal to 9. Solution

agitation was maintained for an additional 30 minutes. Then, the solid was filtered, washed with deionized water and ethanol (Vetec, 95%) and then dried at 100 ºC for 20 hours under static air. The dried material was grinded and sieved to particles smaller than 0.3 mm. Finally, the material was calcined at 500 ºC for 2 hours with a heating rate equal to 2 ºC/min, under air flow (50 mL/min). The sample presented a γ-alumina structure according to powder X-ray diffraction patterns (XRD), and a specific surface area, pore volume and pore size equal to 274.3 m^2/g, 0.23 cm^3/g and 32.8 Å, respectively, calculated from measured N_2 adsorption-desorption isotherms at 77 K (Micromeritics, ASAP2000) [6,45].

NH_3-TPD analysis was carried out in a Chembet-3000 system (Quantachrome Instruments, USA). The NH_3 concentration of the gas effluent was measured in-line with a mass spectrometer (ThermoStar™ Pfeiffer Vacuum Quadrupole, Pfeiffer, USA), by monitoring the signal m/z equal to 16 and subtracting the water interference as further detailed in [6]. Alumina samples (200 mg) were pre-treated *in situ* under nitrogen flow of 19 mL/min at 500 ºC for 1 hour, at heating rate of 10 ºC/min. For the NH_3 adsorption step, the sample temperature was stabilized at 100 ºC before exposition to the gas feed, which consisted of a 5 vol% NH_3/N_2 mixture, flowing at 19 mL/min for 30 min or until sample saturation, as observed by a constant baseline signal. The excess of ammonia was removed with a flow of N_2 for approximately 2 hours or until attainment of a constant baseline signal. Finally, the desorption step was performed by heating the sample at 10 ºC/min from 100 to 677 ºC and maintaining this temperature or 1 hour under a N_2 flow. A good experimental reproducibility of the TPD experimental setup was confirmed by three replicated experiments, as illustrated in Fig. S2 of the *SI*.

Empirical deconvolution quantitative analysis

Deconvolution procedures are usually employed to resolve a curve that contains two or more overlapping peaks using a sum of simpler unimodal curves, which can allow for easier identification and analysis of the thermogram peaks. To perform this task, a family of Gaussian probability distribution functions, Eq. (1), is normally considered [27,46], considering that the sign placed before the summation is positive for TPD and negative for TPR experiments. The subscript $i = 1, \ldots NS$ represents the individual Gaussian curves; A_i represents the area under the individual curve i; and σ_i and $x_{0,i}$ represent the standard deviation (closely related with the peak-width) and the central position of the curve i, respectively.

$$y = y_0 \pm \sum_{i=1}^{NS} \frac{A_i}{\sigma_i \sqrt{2\pi}} \exp\left[-\frac{1}{2}\left(\frac{x - x_{0,i}}{\sigma_i} \right)^2 \right] \quad (1)$$

Several combinations of NS (typically NS ranges from 2 to 5) curves can be tested until attainment of the optimal number of sites that can be used to fit the thermogram signal, y^e, by minimizing the difference between the observed, y^e, and the simulated thermogram response, y. A_i, σ_i, and $x_{0,i}$, $i = 1, \ldots NS$, are the model parameters that must be estimated with the available experimental data. y_0 is the baseline offset: in the TPD experiments, its value is equal to zero, while in the TPR experiments it must be equal to the feed H_2 concentration. Thus, the thermogram deconvolution performed with NS peaks and based on Eq. (1) leads to $3 \times NS$ estimable parameters. Estimation of model parameters was performed as described in Section 2.6.

TPR phenomenological modelling

The mathematical phenomenological modelling of TPR experimental thermograms involved two molar balances: one over the catalyst surface for each reducible species *i*, Eq. (2), and another one for the reducing agent in the gas-phase, Eq. (3).

$$-\frac{dC_{x_i}}{dt} = r_i = k_i P_{H_2}^{p} C_{x_i}^{q} \quad (2)$$

$$C_{H_2}^{in} - C_{H_2} = \frac{M_{Cat}}{v} \sum_{i=1}^{NS} r_i \quad (3)$$

The rate of reduction r_i of species *i* was described as a function of the kinetic constant k_i, which depends on temperature, the concentration of the reducible species C_{x_i} and the partial pressure of hydrogen P_{H_2}, while the reaction orders *p* and *q*, related to the hydrogen partial pressure and the reducible species concentration were fixed at values equal to 1 and 2, respectively. These values were determined after an initial analysis that indicated these orders as the most suitable for describing the experimental thermogram when compared to remaining possible combinations for *p* and *q* as equal to 1 or 2.

For the molar balance of the reducing agent, Eq. (3), the gas-phase composition was assumed to be perfectly uniform across the reactor vessel. Additionally, the steady state hypothesis was assumed to be valid, given the much slower dynamics of the reduction reaction at the catalyst surface. In Eq. (3), M_{Cat} represents the mass of catalyst; *v* denotes the volumetric flowrate; *NS* indicates the number of reducible species; and $C_{H_2}^{in}$ and C_{H_2} represent the H_2 concentration in the reactor feed and output streams, respectively.

The dependence of the reaction rate constant, k_i, on temperature was described with the reparameterized Arrhenius equation, Eq. (4) [47–50], where T is the measured temperature, T_{ref} is a reference temperature, defined as the average temperature of experimental thermogram (equal to 850 K), and E_i is the activation energy of the reduction reaction involving the i^{th} reducible species.

$$k_i = \exp\left[\ln\left(k_{i,Tref}\right) + \frac{E_i}{RT_{ref}} \frac{\left(T - T_{ref}\right)}{T} \right] \quad (4)$$

The $ln(k_{i,Tref})$ constant is related to the pre-exponential factor of the original Arrhenius equation, k_o, according to Eq. (5).

$$\ln\left(k_{i,Tref}\right) = \ln\left(k_{0,i}\right) - \frac{E_i}{RT_{ref}} \quad (5)$$

Due to the observation of three reduction peaks in the experimental thermogram, as it will be discussed later, the presence of three reducible species was considered, resulting in six kinetic parameters that were estimated from the experimental data ($ln(k_{1,Tref})$, E_1, $ln(k_{2,Tref})$, E_2, $ln(k_{3,Tref})$, E_3). However, the initial concentrations of reducible species, $C_{x_{i,0}}$, were also estimated as extra model parameters. Thus, the TPR fitting procedure based on the phenomenological model involved the adjustment of nine parameters. Finally, it must be noted that it was not necessary to model the temperature program because the temperatures used for model calculations were the actual measured values.

TPD phenomenological modelling

The phenomenological modelling of TPD curves also comprised two molar balances [6,45], one for the acidic species at the catalyst surface, Eq. (6), and another one for the gas phase NH_3 concentration, Eq. (7).

$$\frac{d\theta_{i,NH_3}}{dt} = k_{A,i} P_{NH_3} \left(1-\theta_{i,NH_3}\right) - k_{D,i}\theta_{i,NH_3} \quad (6)$$

$$\frac{dC_{NH_3}}{dt} = \frac{-C_{NH_3}}{\tau} + \frac{\left(1-\varepsilon\right)\rho_P}{\varepsilon}\left(-\sum_{i=1}^{NS} N_i \frac{d\theta_{i,NH_3}}{dt}\right) \quad (7)$$

For the adsorbed NH_3 molecules, a kinetic expression used to describe the rates of adsorption and desorption was considered, as presented in Eq. (6), where (1-$\theta_{i,NH3}$) and $\theta_{i,NH3}$ represent the fractions of acidic species of type *i* that are empty or that contain an adsorbed ammonia molecule, respectively. The parameters $k_{A,i}$ and $k_{D,i}$ are the adsorption and desorption kinetic rate constants, respectively, while P_{NH3} represents the ammonia partial pressure.

For the gas phase molar balance, Eq. (7), the variation of NH_3 concentration, C_{NH_3}, along the reactor length was neglected, as the catalyst mass used to perform the experiment was very low. In Eq. (7), τ is the spatial time, defined as the ratio between the volume of the catalyst and the volumetric feed flowrate; ρ_p is the catalyst particle density; ε is the catalyst porosity; and N_i and *NS* represent the specific concentration and the number of distinct types of acidic species, respectively.

The dependence of the adsorption and desorption kinetic constants, $k_{A,i}$ and $k_{D,i}$, on temperature was described with aid of the reparameterized Arrhenius equation, Eq. (4), where the reference temperature was kept constant and equal to the average temperature of the experimental desorption thermogram (equal to 673 K). Finally, the initial conditions for the set of ordinary differential Eqs. (6-7) were fixed at $\theta_{i,NH_3,0}$ equal to one and $C_{NH_{3,0}}$ equal to zero. Thus, the TPD phenomenological model involved the estimation of *4·NS* kinetic parameters, depending on the number of considered *NS* species.

Parameter estimation procedure

The set of ordinary differential equations used to describe both TPR and TPD processes were solved numerically with the help of the DASSL code [51], with relative and absolute tolerances of 10^{-8}. Estimation of model parameters was performed through minimization of the least squares objective function, Eq. (8), where C_i^{exp} and C_i^{mod} represent the concentration of H_2 or NH_3 observed experimentally and simulated by the model, respectively, and *NE* is the number of data points collected from the TPR or TPD experimental curve.

$$F_{obj} = \sum_{i=1}^{NE} \left(C_i^{\exp} - C_i^{\mathrm{mod}} \right)^2 \tag{8}$$

The minimization of Eq. (8) was performed with the aid of a hybrid optimization method [52,53] implemented in Fortran 90, where the initial minimization phase was performed with the Particle Swarm Optimization (PSO) algorithm [54], followed by a second estimation round where the best estimate obtained in the previous phase was used as the initial guess for the Gauss-Newton method [55,56]. At least five minimization trials were performed, using 50 particles and 500 iterations at each numerical run. Convergence was achieved when the relative modification of the objective function was smaller than 10^{-6}.

Statistical significance of model parameters was evaluated with the standard *t-test* [57], with confidence level of 95%. The statistical performance of empirical and phenomenological models was further assessed by the comparison of their prediction variances, σ_m^2, with each other, as defined in accordance to Eq. (9), with the help of the standard *F-test* [56,57]. In Eq. (9), *Npar* represents the number of parameters used in the model to represent the experimental thermogram.

$$\sigma_m^2 = \frac{F_{obj}}{NE - NPar} \tag{9}$$

Results and discussion

H_2-TPR quantitative data analysis

The reduction profile of the TPR analysis of the Ni/SiO_2 catalyst is presented in Fig. 1. Two well-defined H_2 consumption peaks were observed around 20 and 35 minutes (close to 500 and 600 ºC, respectively), which can be attributed to more and less accessible nickel atoms that present weaker and stronger interactions with the support, respectively [58,59]. A third peak with lower intensity was also observed around 50 minutes (around 650 ºC) and can be attributed to nickel species that present even stronger interactions with the support or to nickel silicate species, such as Ni_2SiO_4 or $NiSiO_3$ [58,59].

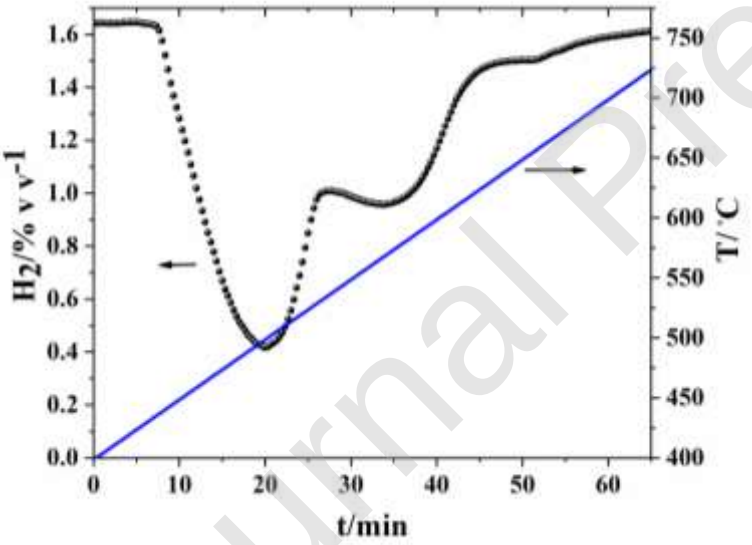

Fig. 1 TPR experimental profile (●) and temperature as a function of time obtained for the Ni/SiO_2 catalyst

The empirical deconvolution model, Eq. (1) with NS of 3, was able to simulate the experimental TPR curve fairly well, as illustrated in Fig. 2, with coefficient of determination, R^2, equal to 0.992, and final objective function value of 0.2324. Although the third peak presented

lower intensity, it was necessary to consider the presence of three reducible sites in order to obtain a good description of the TPR curve, resulting in the fitting of Eq. (1) with 9 parameters, whose estimates are summarized in Table 1 with the respective absolute standard deviations. The relative amounts of each nickel reducible species, F_{NS_i}, are also presented, calculated as the ratio between the peak area related to the i^{th} species and the total area under the curve.

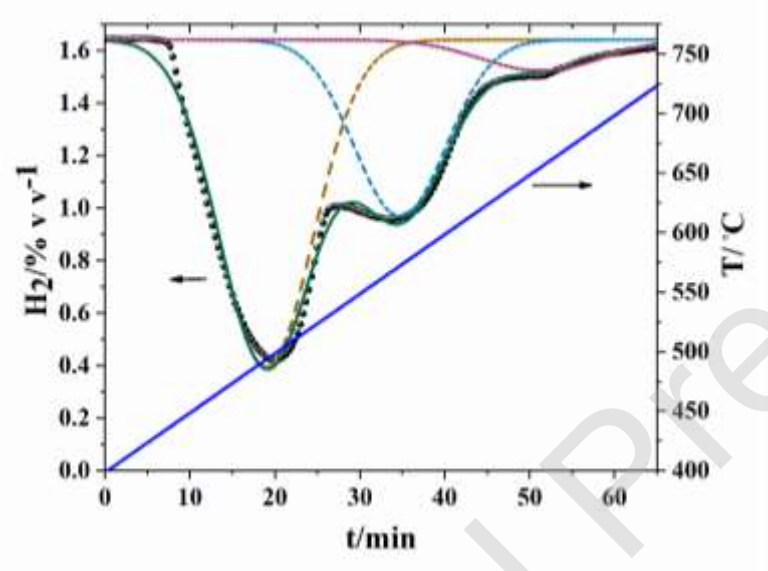

Fig. 2 TPR experimental profile (●), empirical deconvolution model (- and --), Eq. (1) with three Gaussian curves, and temperature as a function of time obtained for the Ni/SiO_2 catalyst

Table 1 Parameter estimates and their standard deviations obtained from the TPR experimental curve (Fig. 1) for the deconvolution model, Eq. (1) with 3 Gaussian curves

Peak (i)	A_i	$x_{0,i}$ (min)	σ_i (min)	F_{NS_i}
1	17.2 ± 0.249	19.0 ± 0.087	5.50 ± 0.075	0.607 ± 0.008
2	9.08 ± 0.472	34.7 ± 0.168	5.38 ± 0.228	0.320 ± 0.017
3	2.07 ± 0.351	51.2 ± 1.303	7.00 ± 1.115	0.073 ± 0.012

F_{obj} [a]	0.2324	R^2	0.992

[a]: defined according with Eq. (8).

Similarly, the TPR phenomenological model, Eq. (2-4) with 3 *NS* reducible species, was also able to describe well the experimental TPR curve, as illustrated in Fig. 3, presenting a coefficient of determination, R^2, equal to 0.996. Although this value was just slightly higher than the one obtained with the empirical model, the final objective function value was equal to 0.1189 in this case, resulting in a model prediction variance, based on Eq. (9), which was almost two times smaller (and statistically different, according to the classical *F-test*) than the one obtained for the empirical model (see Table S1 in the *Supporting Information (SI)*). Therefore, it can be concluded that the phenomenological model provided a statistically better fit to the experimental data compared to the empirical model.

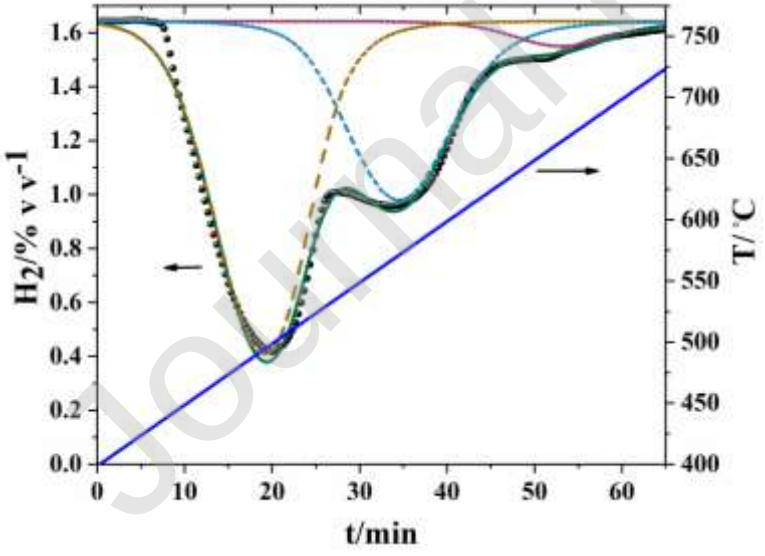

Fig. 3 TPR experimental profile (●), phenomenological model (- and --), Eq. (2-4) with three *NS* reducible species, and temperature as a function of time obtained for the Ni/SiO_2 catalyst

In this case, parameter estimates obtained from the TPR experimental curve are summarized in Table 2, with relative amounts of individual reducible nickel species, F_{NS_i}, calculated as the ratio between the estimated initial concentration of the i^{th} reducible species, $C_{x_{i,0}}$, and the total concentration of reducible species.

Table 2 Parameter estimates and their standard deviations obtained from the TPR experimental curve (Fig. 1) for the phenomenological model, Eq. (2-4) with three *NS* reducible species

Peak (*i*)	$C_{x_{i,0}}$ (mmol/g)	ln($k_{i,Tref}$)[a]	E_i (kJ mol^{-1})	F_{NS_i}
1	0.1267 ± 0.0009	15.476 ± 0.082	398.2 ± 3.6	0.546 ± 0.004
2	0.0941 ± 0.0015	8.793 ± 0.050	264.5 ± 6.6	0.405 ± 0.007
3	0.0112 ± 0.0011	5.237 ± 0.462	371.6 ± 44.3	0.048 ± 0.005
	F_{obj}	0.1189	R^2	0.996

[a]: the units of $k_{i,Tref}$ are g mol^{-1} atm^{-1} s^{-1}.

Whereas parameter estimates obtained with the empirical model, Eq. (1), provided information only about the central position of each peak and the respective peak areas, used to determine the fractions of the reducible species, parameter estimates obtained with the phenomenological model unveiled a much more detailed characterization of the reduction kinetics for the different active species, in addition to the molar fractions of each reducible species. Besides the larger content of information extracted from the phenomenological model, the accuracies of the parameter estimates associated with the amounts of reducible species were also higher when the phenomenological model was employed, as indicated by the smaller standard deviations presented in Table 2 for F_{NS_i} when compared to the values presented in Table

1, suggesting that the use of phenomenological approaches for quantitative TPR analyses can also lead to more precise characterizations of heterogenous catalyst properties.

It is interesting to observe that both empirical and phenomenological models could not provide good representations of the initial stages of reduction, as shown in Figs. 1, 2. In the case of the empirical model, the poor fit of the Gaussian curve in this region could be explained by the less symmetrical shape of the first peak. In the case of the phenomenological model, one should consider that H_2 adsorption at these initial stages may be difficult, since the catalyst surface is composed by oxidized nickel species. When some nickel atoms are reduced, H_2 adsorption can be facilitated, leading to higher rates of reduction and faster decrease of the H_2 concentration [60].

Therefore, in order to account for the above-mentioned process and better describe the kinetics of the reduction reaction for the first reduction peak, the phenomenological model was modified to include the contribution of the reaction between adsorbed H_2 with metallic nickel and nickel oxide sites on the overall rate of reduction of the first reducible species. The reaction rate was described by assuming a system of two consecutive reactions, Eqs. (10-11), where the first H_2 adsorption step is assumed to be in equilibrium, Eq. (10), and the second surface reaction step, Eq. (11), controls the reaction rate according to Eq. (12).

$$H_2 + Ni^0 \rightleftarrows H_2Ni^0 \tag{10}$$

$$H_2Ni^0 + NiO \longrightarrow 2Ni^0 + H_2O \tag{11}$$

$$r = kC_{H_2Ni^0}C_{NiO} \tag{12}$$

As the adsorption of hydrogen is assumed to be in equilibrium, $H_2{\cdot}Ni^0$ concentration can be expressed as a function of the H_2 partial pressure and the metallic nickel concentration, C_{Ni^0}, resulting in the reaction rate described by Eq. (13), where K_{ads} represents the equilibrium constant for the H_2 adsorption step, Eq. (10).

$$r = kK_{ads}P_{H_2}C_{Ni^0}C_{NiO} \quad (13)$$

Consequently, the molar balance for the first reducible species at the catalyst surface can be described in accordance to Eq. (14), where the first term on the right-hand side represents the rate of reduction due to the reaction between H_2 and nickel oxide species, as described previously in Section 2.4, and the second term is the rate of reduction associated with reactions presented in Eqs (10-11), as shown in Eq. (13). However, the metallic nickel concentration, C_{Ni^0}, was inferred as the difference between the initial concentration of reducible species, $C_{x_{1,0}}$ and the remaining concentration of this species at time *t*, C_{x_1}.

$$-\frac{dC_{x_1}}{dt} = r_1 = k_1 P_{H_2} C_{x_1}^2 + k_{1a} P_{H_2} \left(C_{x_1,0} - C_{x_1}\right) C_{x_1} \quad (14)$$

It is important to note that the kinetic constant k_{1a} in Eq. (14) is an apparent kinetic rate constant, since it represents the product between the kinetic rate constant *k* and the H_2 adsorption equilibrium constant K_{ads}, as illustrated in Eq. (13). Additionally, the temperature dependence of the apparent kinetic rate constant k_{1a} can also be described in the form of the reparametrized Arrhenius equation, Eq. (4). Thus, the modified phenomenological model comprised four ordinary differential equations, where the molar balances for the first, second and third reducible species were described by Eq. (14) and (2), respectively, and the H_2 balance for the gas phase was described by Eq. (3), resulting in 11 model parameters to be estimated from the TPR experimental curve: $\ln(k_{1,Tref})$, E_1, $\ln(k_{1a,Tref})$, E_{1a}, $\ln(k_{2,Tref})$, E_2, $\ln(k_{3,Tref})$, E_{3a}, $C_{x1,0}$, $C_{x2,0}$, $C_{x3,0}$.

As expected, the improved phenomenological model was able to simulate the TPR experimental curve with significantly higher statistical quality, as illustrated in Fig. 4, where the much better description of the initial stages of reduction can be clearly visualized. In this case, the coefficient of determination was equal to 0.998 and the final objective function value was

equal to 0.0569. The model prediction variance, Eq. (9), was found to be approximately 2 times lower than the prediction variance obtained with the previous phenomenological model (and 4 times lower than the empirical model variance, as illustrated in Table S1 of the *SI*), indicating that the modification of the reaction rate equation for the first reducible species resulted in an improved version of the model, when compared to the results obtained with the first proposed phenomenological modelling approach.

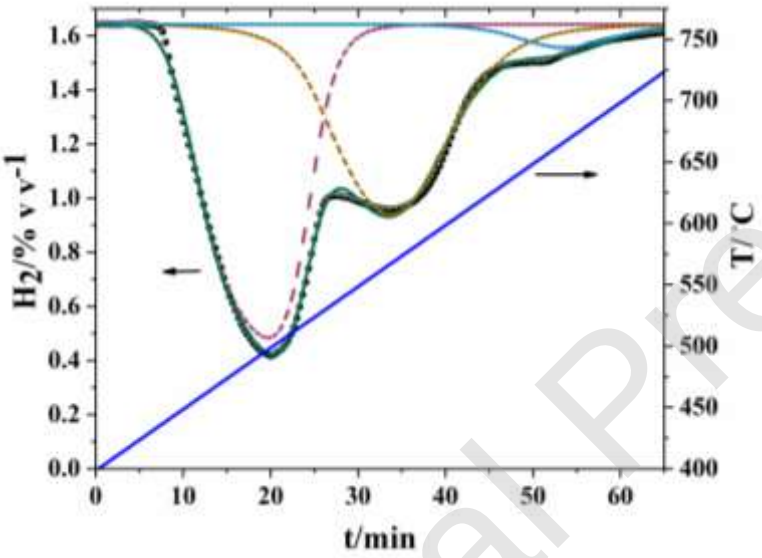

Fig. 4 TPR experimental profile (●), phenomenological model accounting for the autocatalytic reaction contribution on the reduction rate for the first reducible species, Eq. (2-3 and 14), (- and --), and temperature as a function of time obtained for the Ni/SiO_2 catalyst. Note how initial stages of reduction are better described when compared to Fig. 2-3

Thus, the improved description of the TPR experimental curve supports the assumption that the kinetics of reduction during the initial stages can be facilitated by the contribution of the reaction involving H_2 adsorbed on metallic nickel atoms, in accordance with a reaction pathway that resembles an autocatalytic reaction, Eqs. (10-13), in line with previous hypotheses [60,61].

As a result, the accuracies of the parameter estimates related to the relative amounts of individual reducible species, F_{NS_i}, was at least doubled, as illustrated by the smaller standard deviations presented in Table 3, which also summarizes the parameter estimates for the kinetic constants and initial concentrations of reducible species.

Table 3 Parameter estimates and their standard deviations obtained from the TPR experimental curve (Fig. 1) for the phenomenological model accounting for the autocatalytic reaction contribution on the reduction rate for the first reducible species, Eq. (2-3 and 14)

Peak (*i*)	$C_{x_{i,0}}$ (mmol g^{-1})	ln($k_{i,Tref}$)[a]	E_i (kJ mol^{-1})	F_{NS_i}
1	0.1227 ± 0.008	16.494 ± 0.231 <u>8.425 ± 0.096</u>	513.3 ± 14.8 <u>-5.21 ± 5.16</u>	0.532 ± 0.003
2	0.0968 ± 0.0012	8.780 ± 0.036	259.3 ± 4.8	0.420 ± 0.005
3	0.0110 ± 0.0008	5.193 ± 0.334	376.0 ± 31.8	0.048 ± 0.003
	F_{obj}	0.0569	R^2	0.998

[a]: the units of $k_{i,Tref}$ are g mol^{-1} atm^{-1} s^{-1}). Underlined values are the kinetic constants for the autocatalytic reaction (constant k_{1a} from Eq. (13)).

Regarding the activation energy of the kinetic rate constant that describes the first autocatalytic step, a negative value equal to -5.21 kJ/mol was obtained. In fact, considering its high standard deviation, equal to 5.16 kJ/mol, this value was not significantly different from zero and might also be positive. However, it must be emphasized that this is an apparent activation energy, since this parameter represents the product between the kinetic rate constant *k* and the adsorption equilibrium constant K_{eq}. This result can be explained by the fact that H_2 adsorption

onto metallic nickel can decrease with temperature [62], leading to a negative apparent activation energy for this autocatalytic reaction. Consequently, it is not necessary to consider this autocatalytic reaction step in the mechanism that describes the reduction of the second and third reducible species, since the contribution of adsorption can be assumed to become less significant as the temperature increases. Furthermore, the description of reduction kinetics for the second and third reducible species with Eq. (2) was very good, not justifying the inclusion of additional reaction steps, and respective parameters, into the model.

Based on the previous paragraphs, it can be said that quantitative TPR data analyses with the proposed phenomenological approaches should be preferred, instead of using the empirical deconvolution procedures, as the phenomenological technique allowed for quantification of active sites with higher accuracy and provided information about the kinetics of catalyst reduction. Additionally, the phenomenological model can be used to simulate TPR profiles at other operational conditions, guiding the design of experiments that can be carried out to enhance the separation of overlapped peaks, thus also contributing for the quantification of relative amounts of reducible species with even higher precision, as illustrated in Fig. S3 of the *SI*, which presents simulated TPR profiles calculated with different heating rates. However, it should be noted that model simulations as presented in Fig. S3 represent the model behavior only, which should be further confirmed by additional experiments. In this work, to assess how well model predictions could describe TPR experimental profiles at different heating rates, we have compared an additional experiment performed using a heating rate of 15 ˚C/min with model simulations at the same conditions, as illustrated in Fig. S4. As it can be seen, the additional experimental profile was described fairly well by the model simulations, supporting the use of the developed model for TPR quantitative analysis and further design of experiments.

NH_3-TPD experimental data analysis

Fig. 5 shows the TPD experimental profile obtained for the alumina catalyst, where two distinct peaks can be observed: the first one is highly asymmetrical and the second one is nearly symmetrical. The first peak presented a steep slope due to the high rates of ammonia desorption. After reaching a point of maximum, the smooth reduction of the ammonia concentration could be observed. Around 50 minutes, the ammonia concentration in the effluent gas presented a second increase, although not so sharp as the first peak, which was probably due to ammonia desorption from a distinct type of acidic site. It has been commonly accepted that acid sites associated with desorption peaks at higher temperatures are stronger than the ones observed at lower temperatures. NH_3 desorption peaks observed for γ-Al_2O_3 alumina catalysts at lower temperature ranges are usually assigned to Lewis acidic sites related to $Al^{\delta+}$ atoms. Meanwhile, desorption peaks placed at higher temperatures are normally ascribed to Brønsted acidity related to hydroxyl groups or stronger Lewis acid sites [6,63].

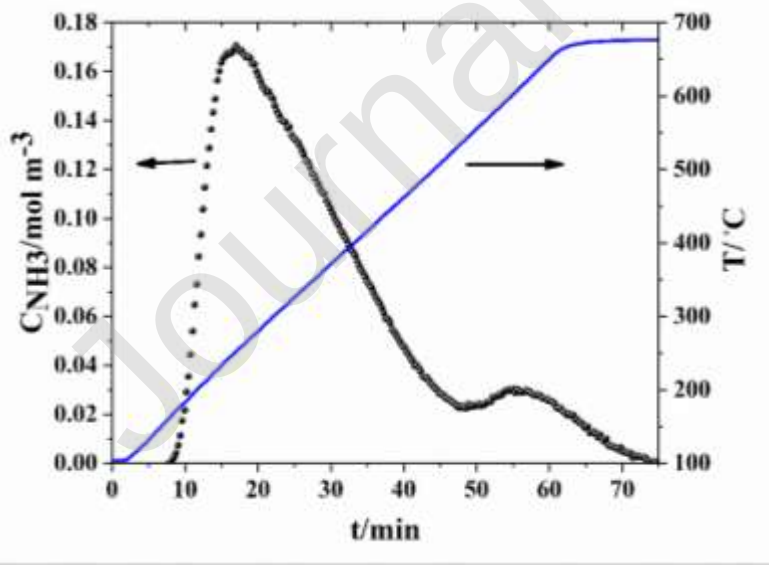

Fig. 5 NH_3-TPD experimental profile (●, left axis) and temperature (-, right axis) as a function of time obtained for the alumina catalyst.

Given the experimental observation of two desorption peaks, the quantitative analysis of the experimental TPD profile was initially evaluated with the empirical modelling approach and two Gaussian curves, as illustrated in Fig. 6 (a). However, in this case, the second experimental peak was not described by the model at all, with the two Gaussian curves being used to describe the first asymmetrical peak, resulting in a poor fit and suggesting that additional Gaussian curves could be needed to provide a reasonable fit. For this reason, the experimental TPD profile was also evaluated with the empirical deconvolution model with 3, 4 and 5 Gaussian curves, as illustrated in Fig. 6 (b-d). When a third Gaussian curve was employed (Fig. 6 (b)), the second experimental peak was described slightly better by the model, but the quality of the overall model simulation was still poor.

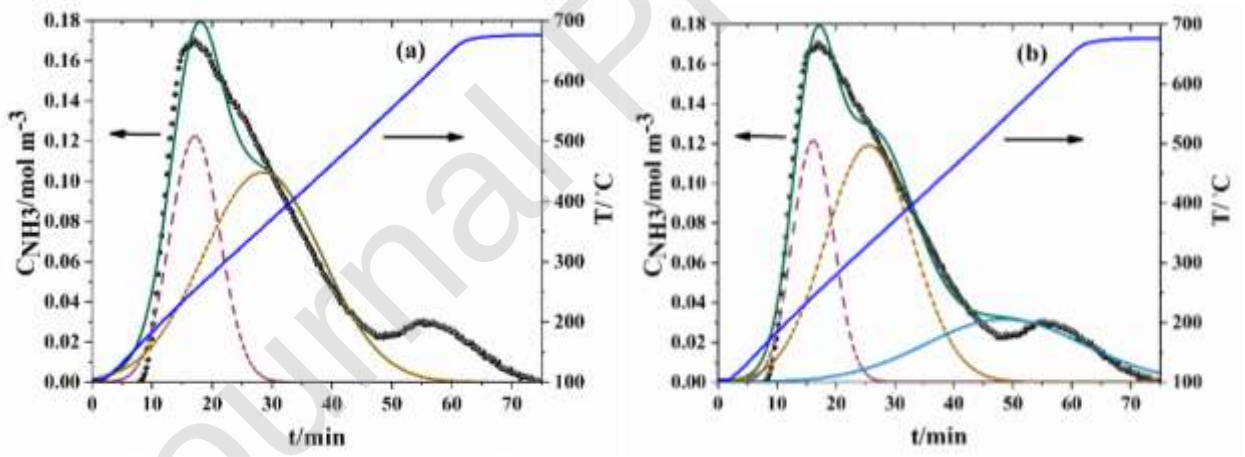

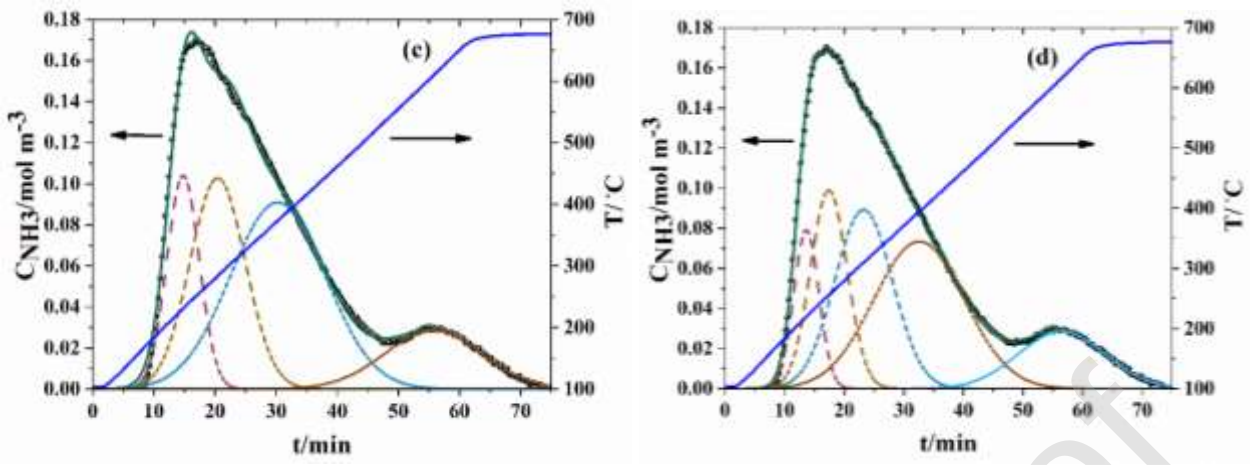

Fig. 6 TPD experimental profile (●) and empirical deconvolution model (- and --), Eq. (1) with 2 (a), 3 (b), 4 (c) and 5 (d) Gaussian curves, as a function of time obtained for the alumina catalyst

By adding a fourth (Fig. 6 (c)) and a fifth (Fig. 6 (d)) Gaussian curve, the quality of the empirical model fit was improved significantly, as also indicated by a significant reduction of the final objective function value, summarized in Table 4 along with the remaining parameter estimation results for each analyzed empirical model. However, although leading to the significant reduction of the final objective function value, the use of 5 Gaussian curves generated poor parameter estimates for peaks 2 and 3, which presented very large standard deviations. In fact, the areas of the peaks 2 and 3 could be regarded as not significantly different from zero, assuming a confidence level of 95 %. Therefore, 4 Gaussian curves could be considered sufficient for proper statistical description of the experimental TPD profile. Consequently, one could conclude that the catalyst contains 4 (or 5, if statistical significance is not considered) different types of acid sites. Additionally, one could also classify the strength of the identified acid sites as weak, medium and strong (and maybe very strong), depending on the respective characteristic peak time (or temperature) [28,64]. It must be advised that this procedure must be

discouraged, since these quantitative (and phenomenological) conclusions are based on results obtained with an empirical model that lacks physical significance.

Table 4 Parameter estimates and their standard deviations obtained from the TPD experimental curve (Fig. 5) for the deconvolution model, Eq. (1) with *NS* acid sites varying from 2 to 5

NS	F_{obj}	R^2	Peak (*i*)	A_i	$x_{0,i}$ (min)	σ_i (min)	F_{NS_i}
2	0.04954	0.939	1	1.27 ± 0.18	17.13 ± 0.15	4.12 ± 0.28	0.329 ± 0.047
			2	2.59 ± 0.20	28.43 ± 0.89	9.86 ± 0.53	0.671 ± 0.047
3	0.01003	0.988	1	1.06 ± 0.11	16.13 ± 0.08	3.48 ± 0.15	0.250 ± 0.027
			2	2.19 ± 0.20	25.65 ± 0.42	7.35 ± 0.41	0.517 ± 0.047
			3	0.99 ± 0.12	48.60 ± 1.81	13.35 ± 1.39	0.233 ± 0.028
4	0.00204	0.997	1	0.69 ± 0.16	14.79 ± 0.10	2.66 ± 0.14	0.165 ± 0.037
			2	1.16 ± 0.41	20.44 ± 0.53	4.50 ± 0.64	0.277 ± 0.097
			3	1.77 ± 0.29	30.30 ± 1.23	7.78 ± 0.72	0.422 ± 0.069
			4	0.57 ± 0.03	55.73 ± 0.40	8.00 ± 0.33	0.136 ± 0.006
5	0.00046	0.998	1	0.42 ± 0.19	13.66 ± 0.19	2.10 ± 0.15	0.100 ± 0.046
			2	0.76 ± 0.52	17.42 ± 0.58	3.06 ± 0.68	0.182 ± 0.124

	3	1.08 ± 0.67	23.25 ± 1.32	4.82 ± 1.11	0.258 ± 0.161
	4	1.40 ± 0.37	32.56 ± 1.90	7.58 ± 0.89	0.335 ± 0.089
	5	0.52 ± 0.02	56.47 ± 0.26	7.28 ± 0.18	0.124 ± 0.004

On the other hand, when the phenomenological modelling approach was considered, just two acid sites were required to represent with good quality the experimental TPD profile, as illustrated in Fig. 7 and Table 5, which summarizes parameter estimates and their respective standard deviations. In this case, the obtained final objective function value was equal to 0.00150, which was smaller than the one obtained with the empirical deconvolution model containing 4 Gaussian curves. Thus, the phenomenological approach supports the hypothesis that both desorption and re-adsorption rates were important to describe the net desorption rate associated with the first acidic site, as the adsorption rate at this site was responsible for the slow reduction of the ammonia concentration in the effluent gas.

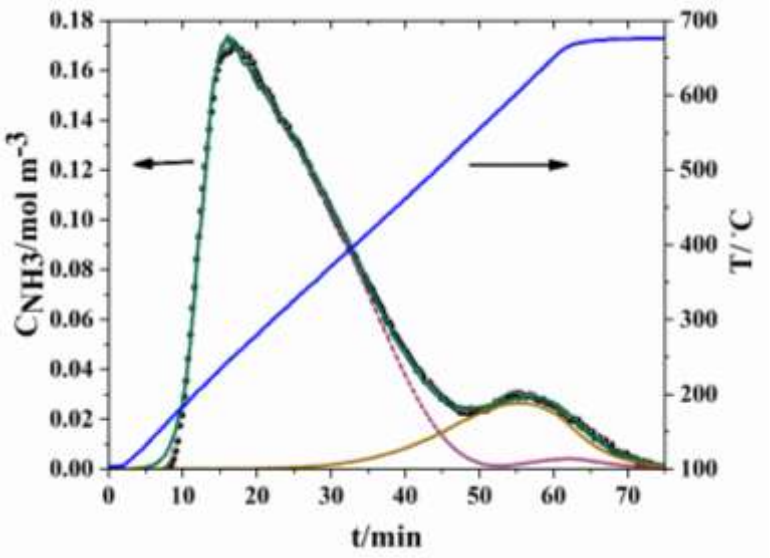

Fig. 7 TPD experimental profile (●) and phenomenological model (- and --), Equations (6-7) with 2 *NS* kind of acid sites, as a function of time obtained for the alumina catalyst. The catalyst particle density, ρ_p, and its porosity, ε, were measured in laboratory and were equal to 0.96 g cm^{-3} and 0.6, respectively

Table 5 Parameter estimates and their standard deviations obtained from the TPD experimental curve (Fig. 5) for the TPD phenomenological model based on 2 *NS* acid sites, Eq. (6-7)

Parameter		Acid site I	Acid site II
N_i (mmol g^{-1})		0.696 ± 0.003	0.162 ± 0.004
ln($k_{D,i,Tref}$) (ln(min^{-1} atm^{-1}))		4.48 ± 0.09	-5.47 ± 0.09
$E_{D,i}$ (kJ mol^{-1})		113.08 ± 1.25	75.93 ± 2.58
ln($k_{A,i,Tref}$) (ln(min^{-1}))		-3.02 ± 0.09	---
$E_{A,i}$ (kJ mol^{-1})		73.05 ± 1.08	---
F_{NS_i}		0.811 ± 0.004	0.189 ± 0.004
F_{obj}	0.00150	R^2	0.998

Additionally, the differences between activation energies for adsorption (73.1 $kJ \cdot mol^{-1}$) and desorption (113.1 $kJ \cdot mol^{-1}$) were negative, indicating as expected that the net adsorption process is exothermic. In contrast, parameter values related to re-adsorption in the second acid site were not statistically significant, probably due to the lower importance of re-adsorption at higher temperatures, resulting in also no significant improvement in the model fit quality when re-adsorption is assumed to occur on both sites simultaneously, as illustrated in Fig. S5 and Table S2 in the *SI*. However, when re-adsorption is neglected on both catalyst sites, much poorer model fits are obtained, as illustrated in Figure S6 and Table S3. It can be observed that desorption peaks are approximately symmetrical and cannot provide appropriate description of the first desorption peak when re-adsorption is neglected on both sites.

It is also interesting to observe that, when ammonia release started in the second acid site, the rate of desorption from the first site was reduced, since ammonia released from the second site increased the rate of adsorption at the first site, reducing the net desorption rate from this site. This behavior can also be visualized in Fig. 7 around 53 min, as the ammonia concentration from the first acid site reached a minimum value which was subsequently increased due to the adsorption of ammonia released from the second acid site, resulting in a second maximum value around 62 min, which was then reduced until desorption of the remaining amount of ammonia. Consequently, the observed second peak presented contributions from both acid sites, a process which could only be detected due to the use of the phenomenological model and could not be explained by the empirical modelling approaches.

Additionally, the proposed analysis also places a question mark on the common agreement that desorption peaks observed at higher temperatures are related to stronger acidic sites, when compared to the ones observed at lower temperatures, as indicated by the smaller activation energy estimated for the second acid site (75.9 $kJ \cdot mol^{-1}$) when compared to the first

one (113.1 $kJ \cdot mol^{-1}$), Table 5. It is important to note that these results have been confirmed by the analysis of a series of distinct alumina catalysts which have been prepared using different thermal treatments [6], as illustrated in Fig. S7, which further demonstrates the validity of the phenomenological modelling approach by the comparison of model simulations, using kinetic parameters as described in Table 5, and experimental profiles obtained for three additional and distinct alumina catalysts. As it can be seen, obtained model simulations can be regarded as excellent.

Therefore, we hope that the reader will be convinced of the many advantages provided by the use of the phenomenological model approach for quantitative analyses of TPD experiments, as it allows the meaningful determination of the number of distinct active sites and their relative quantities and also provide information on the kinetic behavior of desorption. Moreover, the phenomenological approach also allows the analysis of the effect of experimental conditions, like the temperature program, on the kinetics of NH_3 desorption, as other temperature values can be used as inputs to perform model simulations, while similar studies cannot be performed with the empirical approach, which only considers the ammonia concentration in the effluent gas and does not provide information about the kinetic behavior of the catalyst sites.

Conclusions

Although temperature-programmed (TP) techniques have been widely used for the characterization of heterogeneous catalysts for decades, the quantitative analysis of TP data remains mostly limited to empirical modelling techniques, particularly in TPR and TPD experiments. Thus, the present work has evaluated the use of phenomenological modelling approaches for quantitative analysis of TP experiments when compared to results obtained by empirical deconvolution procedures.

For TPR, the phenomenological modelling led to hydrogen consumption peaks for each reducible species that presented shapes similar, to some extent, to empirical Gaussian curves. However, the fitting obtained with the phenomenological model proved to be statistically better than the one obtained with the empirical deconvolution model, leading to more accurate estimates of the relative concentration of reducible species. Furthermore, the phenomenological model allowed the extraction of physicochemical information that could not be provided by the conventional empirical deconvolution procedure, particularly in respect to the kinetics of the reduction reaction. In this case, when the role of the initial reduced nickel atoms on the reduction kinetics was taken into account, by facilitating H_2 adsorption and thus increasing the reduction rate of adjacent oxidized nickel atoms, much better fit of the experimental data could be obtained, as the rapid increase in the initial hydrogen consumption could be more satisfactorily explained.

When the TPD analysis was considered, the asymmetric shape of the experimental adsorption/desorption peak artificially required the assumption of up to four distinct active acidic sites on the alumina catalyst surface in order to describe the TPD profile appropriately with the empirical deconvolution model. On the other hand, the phenomenological model supported the existence of only two distinct acid sites, as the asymmetric shape of the desorption peak could be explained by occurrence of re-adsorption. Besides suggesting a more meaningful value for the number of distinct acidic sites, the use of the phenomenological model provided information about the desorption kinetics, placing also a question mark on the common hypothesis that desorption peaks observed at higher temperatures are always related to stronger acidic sites.

We hope this work can contribute for the better development, design and optimization of heterogenous catalysts in order to maximize the efficiency of industrial catalytic processes.

Compliance with ethical standards

Conflict of Interest The authors declare that they have no conflict of interest.

Acknowledgement

The study was financed in part by Conselho Nacional de Desenvolvimento Científico e Tecnológico – Brasil (CNPq) and by Coordenação de Aperfeiçoamento de Pessoal de Nível Superior – Brasil (CAPES) – Finance Code 001.

References

[1] J.W. Chorkendorff I.; Niemantsverdriet, Concepts of Modern Catalysis and Kinetics, Wiley-VCH Verlag GmbH &Co.KGaA, Weinheim, 2003.

[2] T.K. Phung, G. Garbarino, J. Ind. Eng. Chem. 47 (2017) 288–96. 10.1016/j.jiec.2016.11.045.

[3] T. Lever, P. Haines, J. Rouquerol, E.L. Charsley, P. Van Eckeren, D.J. Burlett, Pure Appl. Chem. 86(4) (2014) 545–53. 10.1515/pac-2012-0609.

[4] S. Da Ros, R.S. Braido, N.L. de Souza e Castro, A.L.T. Brandão, M. Schwaab, J.C. Pinto, J. Anal. Appl. Pyrolysis 144 (2019) 104706. 10.1016/j.jaap.2019.104706.

[5] S. Da Ros, M.D. Jones, D. Mattia, J.C. Pinto, M. Schwaab, F.B. Noronha,S.A. Kondrat, T.C. Clarke, S.H. Taylor, ChemCatChem 8(14) (2016) 2376–86. 10.1002/cctc.201600331.

[6] S. Da Ros, E. Barbosa-Coutinho, M. Schwaab, V. Calsavara, N.R.C. Fernandes-Machado, Mater. Charact. 80 (2013) 50–61. 10.1016/j.matchar.2013.03.005.

[7] S. Da Ros, M.D. Jones, D. Mattia, M. Schwaab, E. Barbosa-Coutinho, R.C. Rabelo-Neto, F.B. Noronha, J.C. Pinto, Chem. Eng. J. 308 (2017) 988–1000. 10.1016/j.cej.2016.09.135.

[8] L. Santamaria, G. Lopez, A. Arregi, M. Artetxe, M. Amutio, J. Bilbao, M. Olazar, J. Ind. Eng. Chem. 91 (2020) 167–81. 10.1016/j.jiec.2020.07.050.

[9] P.N. Kechagiopoulos, J.W. Thybaut, G.B. Marin, Ind. Eng. Chem. Res. 53(5) (2014) 1825–40. 10.1021/ie403160s.

[10] S. Bhatia, J. Beltramini, D.D. Do, Catal. Today 7(3) (1990) 309–438. 10.1016/0920-5861(90)87001-J.

[11] J.M. López, A.L. Gilbank, T. García, B. Solsona, S. Agouram, L. Torrente-Murciano, Appl. Catal. B Environ. 174–175 (2015) 403–12. 10.1016/j.apcatb.2015.03.017.

[12] J.M. Kanervo, A.O.I. Krause, J. Phys. Chem. B 105(40) (2001) 9778–84. 10.1021/jp0114079.

[13] D.L. Bhering, M. Nele, J.C. Pinto, V.M.M. Salim, Appl. Catal. A Gen. 234(1–2) (2002) 55–64. 10.1016/S0926-860X(02)00198-9.

[14] P. Heidebrecht, V. Galvita, K. Sundmacher, Chem. Eng. Sci. 63(19) (2008) 4776–88. 10.1016/j.ces.2007.10.012.

[15] N.M. Russell, J.G. Ekerdt, Surf. Sci. 364(2) (1996) 199–218. 10.1016/0039-6028(96)00593-6.

[16] J.M. Kanervo, K.M. Reinikainen, A.O.I. Krause, Appl. Catal. A Gen. 258(2) (2004) 135–44. 10.1016/j.apcata.2003.08.019.

[17] J.M. Kanervo, A.O.I. Krause, J.R. Aittamaa, P.H. Hagelberg, K.J.T. Lipiäinen, I.H. Eilos, J.S. Hiltunen, V.M. Niemi, Chem. Eng. Sci. 56(4) (2001) 1221–7. 10.1016/S0009-2509(00)00343-2.

[18] X. Xian, C. Ran, C. Nai, P. Yang, S. Zhao, L. Dong, Appl. Catal. A Gen. 547(August) (2017) 37–51. 10.1016/j.apcata.2017.08.023.

[19] M. Niwa, N. Katada, K. Okumura, Characterization and Desing of Zeolites Catalysts - Solid acidity, shape selectivity and loading properties, Vol. 141, Springer, London, New York, 2010.

[20] A.S. Al-Dughaither, H. De Lasa, Ind. Eng. Chem. Res. 53(40) (2014) 15303–16. 10.1021/ie4039532.

[21] L. Rodríguez-González, F. Hermes, M. Bertmer, E. Rodríguez-Castellón, A. Jiménez-

López, U. Simon, Appl. Catal. A Gen. 328(2) (2007) 174–82. 10.1016/j.apcata.2007.06.003.
[22] R.J. Cvetanović, Y. Amenomiya, Adv. Catal. 17 (1967) 103–49. 10.1016/S0360-0564(08)60686-0.
[23] W.H. Press, B.P. Flannery, S.A. Teukolsky, W.T. Vetterling, Numerical Recipes in FORTRAN: The Art of Scientific Computing, 2nd ed., Cambridge University Press, Cambridge ; New York, 1992.
[24] H.P.J. Calo J.M., in: E. P. Lahaye J. (Ed.), Fundamental Issues in Control of Carbon Gasification Reactivity, Kluwer Academic Publishers, Dordrecht, 1991, pp. 329–68.
[25] J.H. Zhou, Z.J. Sui, J. Zhu, P. Li, D. Chen, Y.C. Dai, W.K. Yuan, Carbon N. Y. 45(4) (2007) 785–96. 10.1016/j.carbon.2006.11.019.
[26] A. Tanksale, J.N. Beltramini, J.A. Dumesic, G.Q. Lu, J. Catal. 258(2) (2008) 366–77. 10.1016/j.jcat.2008.06.024.
[27] D.L. Hoang, T.T.H. Dang, J. Engeldinger, M. Schneider, J. Radnik, M. Richter, A. Martin, J. Solid State Chem. 184(8) (2011) 1915–23. 10.1016/j.jssc.2011.05.042.
[28] D.L. Carvalho, R.R. De Avillez, M.T. Rodrigues, L.E.P. Borges, L.G. Appel, Appl. Catal. A Gen. 415–416 (2012) 96–100. 10.1016/j.apcata.2011.12.009.
[29] M. Bahmani, B. Vasheghani Farahani, S. Sahebdelfar, Appl. Catal. A Gen. 520 (2016) 178–87. 10.1016/j.apcata.2016.04.018.
[30] Y.P. Tian, X.M. Liu, M.J. Rood, Z.F. Yan, Appl. Catal. A Gen. 545(July) (2017) 1–9. 10.1016/j.apcata.2017.07.022.
[31] J.M. Kanervo, T.J. Keskitalo, R.I. Slioor, A.O.I. Krause, J. Catal. 238(2) (2006) 382–93. 10.1016/j.jcat.2005.12.026.
[32] J.M. Kanervo, S. Kouva, K.J. Kanervo, R. Kolvenbach, A. Jentys, J.A. Lercher, Chem. Eng. Sci. 137 (2015) 807–15. 10.1016/j.ces.2015.07.032.
[33] D.A.M. Monti, A. Baiker, J. Catal. 83(2) (1983) 323–35. 10.1016/0021-9517(83)90058-1.
[34] K. Ehrhardt, M. Richter, U. Roost, G. Öhlmann, Appl. Catal. 17 (1985) 23–45.
[35] J. Schittkowski, D. Buesen, K. Toelle, M. Muhler, Catal. Letters 146(5) (2016) 1011–7. 10.1007/s10562-016-1712-y.
[36] D. Du, J. Kullgren, B. Kocmaruk, K. Hermansson, P. Broqvist, J. Catal. 384 (2020) 252–9. 10.1016/j.jcat.2019.12.042.
[37] T. Gambu, R. Abrahams, E. van Steen, Catalysts 9(4) (2019) 310. 10.3390/catal9040310.
[38] C. Bornes, J.A. Amelse, M. Peacock, C.L. Marshall, M.M. Schwartz, C.F.G.C. Geraldes, J. Rocha, L. Mafra, Eur. J. Inorg. Chem. 2020(19) (2020) 1860–6. 10.1002/ejic.202000050.
[39] H.E. Kissinger, J. Res. Natl. Bur. Stand. (1934). 57(4) (1956) 217–21. 10.1002/9781119959809.ch9.
[40] H.E. Kissinger, Anal. Chem. 29(11) (1957) 1702–6. 10.1021/ac60131a045.
[41] B. Janković, B. Adnadević, S. Mentus, Chem. Eng. Sci. 63(3) (2008) 567–75. 10.1016/j.ces.2007.09.043.
[42] P.A. Redhead, Vacuum 12(July) (1962) 203–11. 10.1016/0042-207X(62)90978-8.
[43] D.L. Silva, Preparação de Catalisadores de Ni/SiO_2 - Estudo Simultâneo das Etapas de Precipitação e Redução. PhD thesis, Federal University of Rio de Janeiro, 1999.
[44] M. Nele, A. Vidal, D.L. Bhering, J.C. Pinto, V.M.M. Salim, Appl. Catal. A Gen. 178(2) (1999) 177–89. 10.1016/S0926-860X(98)00285-3.
[45] S. Da Ros, Produção de eteno a partir de etanol utilizando aluminas. Federal University of Santa Maria, 2012.
[46] J. Pitha, R.N. Jones, Can. J. Chem. 44 (1966) 3031–50. 10.1139/v66-445.

[47] M. Schwaab, J.C. Pinto, Chem. Eng. Sci. 62(10) (2007) 2750–64. 10.1016/j.ces.2007.02.020.
[48] M. Schwaab, L.P. Lemos, J.C. Pinto, Chem. Eng. Sci. 63(11) (2008) 2895–906. 10.1016/j.ces.2008.03.010.
[49] D.G. Watts, Can. J. Chem. Eng. 72(4) (1994) 701–10. 10.1002/cjce.5450720420.
[50] G.E.P. Box, Ann. N. Y. Acad. Sci. 86(3) (1960) 792–816. 10.1111/j.1749-6632.1960.tb42843.x.
[51] L.R. Petzold, IMACA World Congress, Montreal, 1982, pp. 1–11.
[52] M. Schwaab, J. Biscaia E.C., J.L. Monteiro, J.C. Pinto, E.C. Biscaia Júnior, J.L. Monteiro, J.C. Pinto, E.C. Biscaia, J.L. Monteiro, J.C. Pinto, Chem. Eng. Sci. 63(6) (2008) 1542–52. 10.1016/j.ces.2007.11.024.
[53] M. Schwaab, A.L. Alberton, J.C. Pinto, ESTIMA&PLANEJA: Pacote computacional para estimação de parâmetros e de planejamento de experimentos, Rio de Janeiro, 2010.
[54] J. Kennedy, R. Eberhart, Proceedings of ICNN'95 - International Conference on Neural Networks, Vol. 4, IEEE, 1995, pp. 1942–8.
[55] M. Schwaab, J.C. Pinto, Análise de Dados Experimentais I: Fundamentos de Estatística e Estimação de Parâmetros, e-Papers, Rio de Janeiro, 2007.
[56] S. Da Ros, M. Schwaab, J.C. Pinto, Ref. Modul. Chem. Mol. Sci. Chem. Eng. (2017). 10.1016/B978-0-12-409547-2.13918-6.
[57] G.E.P. Box, J.S. Hunter, W.G. Hunter, Statistics for Experimenters. Design, Innovation, and Discovery., second ed., John Wiley & Sons, New Jersey, 2005.
[58] F. Pompeo, N.N. Nichio, M.G. González, M. Montes, Catal. Today 107–108 (2005) 856–62. 10.1016/j.cattod.2005.07.024.
[59] W.K. Jóźwiak, M. Nowosielska, J. Ryczkowski, Appl. Catal. A Gen. 280(2) (2005) 233–44. 10.1016/j.apcata.2004.11.003.
[60] J. Bandrowski, C.R. Bickling, K.H. Yang, O.A. Hougen, Chem. Eng. Sci. 17(5) (1962) 379–90. 10.1016/0009-2509(62)80039-6.
[61] A.F. Benton, P.H. Emmett, J. Am. Chem. Soc. 46(12) (1924) 2728–37. 10.1021/ja01677a018.
[62] E.B. Maxted, N.J. Hassid, Trans. Faraday Soc. 28 (1932) 253–61.
[63] L. Martins, D. Cardoso, P. Hammer, T. Garetto, S.H. Pulcinelli, C. V. Santilli, Appl. Catal. A Gen. 398(1–2) (2011) 59–65. 10.1016/j.apcata.2011.03.014.
[64] Y. Shi, X. Li, X. Rong, B. Gu, H. Wei, Y. Zhao, W. Wang, C. Sun, Catal. Letters (0123456789) (2020). 10.1007/s10562-020-03115-0.